

# PREDICTIVE CONTROL OF SPATIAL FLEXIBLE MECHANISMS

Erfan Shojaei Barjuei      Alessandro Gasparetto

Department of Electric, Managerial and Mechanical Engineering, University of Udine, Italy

## ABSTRACT

In this paper, position control and reduction of vibration of a 3D flexible L-shape mechanism has been achieved through the synthesis of a constrained Model Predictive Control (MPC). A finite element model, based on the equivalent rigid link system (ERLS) theory, is used in order to describe accurately the dynamic behaviour of the system. The model has been validated through the experimental tests. In order to apply the constrained MPC control on the mechanism, a linearized model which takes gravity force into account is derived as well as a Kalman state estimator. The effectiveness and robustness of the control system has been evaluated and discussed through several tests. Furthermore, the performance of the MPC control has been compared with the performance of classical industrial control (PID).

Keywords: predictive control, flexible-link mechanisms, vibration control

## 1 INTRODUCTION

Modelling, analysing and controlling of flexible mechanisms have been under investigations for about four decades. Moreover, the consequence of accurate modelling and controlling the phenomena of mechanical vibration in flexible mechanisms is designing and fabricating lighter robot manipulators, which is a very important factor of lower operation cost and as well as high operation speed. Several studies have been done in order to define and present a precise mathematical model for flexible multi-body systems. These studies have started with investigation on a single flexible-link mechanisms, after with consideration flexible multi-body mechanisms in a planer and finally flexible mechanisms in the spatial environment [1–5]. The most used and adopted methods for modelling the flexible mechanism includes the usage of discretization methods such as finite element method (FEM) with the purpose of presenting dynamics models using a finite number of elastic degree-of-freedom. Models of such a kind, providing a nodal representation of the mechanism, have been proposed. Some author have also proposed description of flexible mechanisms making use of modal coordinates in place of physical coordinates. [6–9]

The available literature on model-based control strategies for flexible-link mechanisms is often the result of application of modal dynamic models, and less frequently on finite element-based models. Comprehensive reviews of the large number of available works can be found in [5] and [10].

Either linear or nonlinear control schemes have been developed. Linear control schemes have been utilized mostly. Some notable examples are robust control by Caracciolo [11] and sliding mode control by Kurode [13]. Also several works have proposed the use of Model Predictive Control (MPC) as an effective and suitable solution to the problem of damping vibration in flexible link mechanisms and structure. An experimental validation of MPC as position and vibration control is available in [20]. The mechanism under consideration is a single-link, and control is achieved on a relatively slow sampling frequency. A good overview of the topic, with several applicative example, is available in [21]. Other kind of mechanisms have been investigated by Boscarol for five bar link mechanism in [12] and four bar link mechanism in [23].

Currently, to the best of authors' knowledge, there are no available works on the predictive control of spatial flexible-link mechanisms. It should be mentioned that the majority of works in this area are application to planar mechanisms, often moving in the horizontal plane, thus without taking into account gravity. The aim of this paper is also to provide a feasible solution that can deal with the nonlinearities imposed by the presence of gravity force.

---

Contact author: Alessandro Gasparetto<sup>1</sup>

<sup>1</sup>DIEGM, University of Udine  
Via delle Scienze, 208 - 33100 Udine, Italy

In this paper model predictive control (MPC) with constrains is proposed to control the position and minimize the amplitude the mechanical vibration during the motion of a 3D flexible L-shape mechanism. There are some motivating reasons for choosing this controller: first, the prediction ability based on an internal model can be a very effective advantages in fast-dynamic systems. Then MPC is well applicable to MIMO plants, because the outputs are calculated by solving a minimization problem which can take in consideration of several variables. Another remarkable advantages of this control scheme is its competences to perform constrains on both control and controlled variables [14].

The linearized model which is used in the MPC controller scheme is based on equivalent rigid-link system (ERLS) theory which is developed and proposed by Vidoni in [15]. The spatial flexible L-shape mechanism is taken into consideration in this work as a test bench mechanism, while having a single degree of freedom and allows 3D motion and elastic displacement.

The paper is organized as follows: Section 2 briefly explains the mathematical model of flexible mechanism, which is valid for any spatial flexible multi-body system. The description of the reference mechanism is given in Section 3. Section 4 provides a description on the linearization procedure as well as the accuracy validation and designing procedure of Kalman state estimator. A brief description of synthesis of model predictive control is presented in the Section 5. In Section 6 simulation results obtained controlling the nonlinear system with the MPC controller have been discussed. An evaluation of robustness properties of the controller is provided by several tests in Section 7. In Section 8 the results of a comparison between the performance of proposed MPC controller and a classical PID controller are presented.

## 2 DYNAMICS MODEL OF A 3D FLEXIBLE MECHANISM

One of the most studied topics in flexible multi-body systems is dynamic modelling which is still an open issue to investigate. In comparison with rigid mechanisms, the elastic behaviour of flexible mechanism makes the mathematical formulation of the models, which influence and regulate the real physical behaviour of the system, quite complex.

The approach used here for modelling of the systems with large displacements and small elastic deformation is based on Equivalent Rigid Link System (ERLS) concepts which first was introduced for a planer mechanisms by Giovagnoni in [3], and then expanded to 3D environment by Vidoni in [15,22] which is briefly explained in this section .

One of the main advantages of the ERLS approach in is that the standard mechanisms definitions and concepts of 3D kinematics could be adopted to formulate and solve the ERLS dynamic model.

### 2.1 Kinematics

As shown in Figure 1, each flexible link of the mechanism can be divided into finite elements. Being  $\{X, Y, Z\}$  a constant

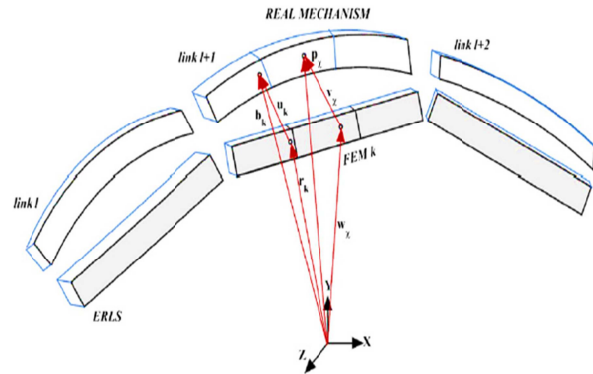


Figure 1 Kinematic definition of the ERLS

global reference frame, let us consider  $u_i$  and  $r_i$  as the vector of the nodal elastic displacements of the  $i$ -th finite element and the vector of nodal position and orientation for the  $i$ -th element of the ERLS, respectively. Moreover position vector of the generic point of the  $i$ -th element of the ERLS and its elastic displacement are  $w_i$  and  $v_i$  respectively. Hence, the absolute nodal position and orientation of the  $i$ -th finite element  $b_i$  with respect to the global reference frame is:

$$b_i = r_i + u_i \quad (1)$$

The absolute position  $p_i$  of generic point inside the  $i$ -th finite element is:

$$p_i = w_i + v_i \quad (2)$$

For each finite element  $\{x_b, y_b, z_b\}$  is the local reference frame that follows the ERLS motion. Given this, it can be defined a block-diagonal global-to-local transformation matrix  $T_i(q)$  and a local-to-global transformation matrix  $R_i(q)$  can be defined. Therefore it is possible to reform Equation 2 as follows:

$$p_i = w_i + R_i(q)N_i(x_i, y_i, z_i)T_i(q)u_i \quad (3)$$

Where  $N_i(x_b, y_b, z_b)$  is the shape function matrix for the interpolation of the  $i$ -th finite element defined in local frame, and  $q$  is the vector of the generalized coordinates.

It can demonstrated that the expression for the virtual displacement  $\delta p_i$  in the constant reference frame is:

$$\delta p_i = R_i(q)N_i(x_i, y_i, z_i)T_i(q)\delta r_i \delta R_i(q)N_i(x_x, y_x, z_x)T_i(q)u_i + R_i(q)N_i(x_x, y_x, z_x)\delta T_i(q)u_i + R_i(q)N_i(x_x, y_x, z_x)T_i(q)\delta u_i \quad (4)$$

Twice differentiating Equation 3 leads to the expression of the acceleration of a generic point inside the  $i$ -th finite element as:

$$\begin{aligned} \dot{p}_i = & R_i(q)N_i(x_i, y_i, z_i)T_i(q)\dot{r}_i + R_i(q)N_i(x_i, y_i, z_i)T_i(q)\dot{u}_i + \\ & 2\left(\dot{R}_i(q)N_i(x_i, y_i, z_i)T_i(q) + R_i(q)N_i(x_i, y_i, z_i)\dot{T}_i(q)\right)\dot{u}_i + \\ & (\ddot{R}_i(q)N_i(x_i, y_i, z_i)T_i(q) + 2\dot{R}_i(q)N_i(x_i, y_i, z_i)\dot{T}_i(q) + \\ & R_i(q)N_i(x_i, y_i, z_i)\ddot{T}_i(q))u_i \end{aligned} \quad (5)$$

If the kinematic entities of all the finite elements are gathered into one vector, differentiating Equation 1 with respect to time leads to:

$$db = du + dr \quad (6)$$

The configuration of the ERLS (as well as its velocity and acceleration) basically depends upon on the vector  $q$  of the free coordinates. This can be reformulated as:

$$dr = S(q)dq \quad (7)$$

$S(q)$  is the matrix of the sensitivity coefficients for all the nodes. Finally, by substituting Equation 7 into Equation 6 the following equation in matrix form can be obtained:

$$db = \begin{bmatrix} I & S_{in} \\ 0 & S_0 \end{bmatrix} \begin{bmatrix} du_{in} \\ dq \end{bmatrix} \quad (8)$$

## 2.2 Dynamics

The dynamic equations of the system can be obtained by applying the principle of virtual works:

$$\delta W^{inertia} + \delta W^{elastic} + \delta W^{external} = 0 \quad (9)$$

which can also be written as:

$$\begin{aligned} \sum_i \delta u_i^T M_i (\ddot{r}_i + \ddot{u}_i) + 2 \sum_i \delta u_i^T (M_{G1i} + M_{G2i}) \dot{u}_i + \\ \sum_i \delta u_i^T (M_{C1i} + 2M_{C2i} + M_{C3i}) u_i + \sum_i \delta u_i^T K_i u_i = \\ \sum_i \delta u_i f_{gi} + \delta u^T f \end{aligned} \quad (10)$$

in which the mass matrix of the  $i$ -th element is:

$$\int_{v_i} T_i^T N_i^T R_i^T R_i N_i T_i \rho_i dv = M_i \quad (11)$$

The stiffness matrix of the  $i$ -th element is:

$$\int_{v_i} T_i^T B_i^T D_i B_i T_i dv = K_i \quad (12)$$

The vector of the equivalent nodal loads due to gravity is:

$$\int_{v_i} T_i^T N_i^T R_i^T g \rho_i dv = f_{gi} \quad (13)$$

The Coriolis terms are related to:

$$\int_{v_i} T_i^T N_i^T R_i^T \dot{R}_i N_i T_i \rho_i dv = M_{G1i} \quad (14)$$

$$\int_{v_i} T_i^T N_i^T R_i^T R_i N_i \dot{T}_i \rho_i dv = M_{G2i} \quad (15)$$

The centrifugal stiffness terms are:

$$\int_{v_i} T_i^T N_i^T R_i^T \ddot{R}_i N_i T_i \rho_i dv = M_{C1i} \quad (16)$$

$$\int_{v_i} T_i^T N_i^T R_i^T 2\dot{R}_i N_i \dot{T}_i \rho_i dv = 2M_{C2i} \quad (17)$$

$$\int_{v_i} T_i^T N_i^T N_i \ddot{T}_i \rho_i dv = M_{C3i} \quad (18)$$

Being  $\delta\Phi_i$  the block-diagonal matrix which contains the virtual angular displacement and  $B_i$  the strain displacement matrix, the following equations holds:

$$\delta T_i^T = \delta\Phi_i T_i^T \quad (19)$$

Since the virtual nodal elastic displacements  $\delta u$  and virtual displacement of the ERLS  $\delta r$  are independent from each other and taking into account the damping through Rayleigh model using  $\alpha$  and  $\beta$  damping constants, Equation 10 can be subdivided in two equations:

$$M(\ddot{r} + \ddot{u}) + 2(M_{G1} + M_{G2})\dot{u} + \alpha M\dot{u} + \beta K\dot{u} + (M_{C1} + 2M_{C2} + M_{C3})u + Ku = f_g + f \quad (20)$$

$$S^T M(\ddot{r} + \ddot{u}) + 2S^T(M_{G1} + M_{G2})\dot{u} + \alpha S^T M\dot{u} + S^T(M_{C1} + 2M_{C2} + M_{C3})u = S^T(f_g + f) \quad (21)$$

Dynamic equations, after the substitution of the second order differential equations of the ERLS, can be grouped and rearranged in matrix form after discarding the equations for elastic degrees of freedom that have been zeroed:

$$\begin{bmatrix} M & MS \\ S^T M & S^T MS \end{bmatrix} \begin{bmatrix} \ddot{u} \\ \ddot{q} \end{bmatrix} = \begin{bmatrix} -2(M_{G1} + M_{G2}) - \alpha M - \beta K & -MS & -(M_{C1} + 2M_{C2} + M_{C3}) - K \\ S^T(-2(M_{G1} + M_{G2}) - \alpha M) & -S^T MS & -S^T(M_{C1} + 2M_{C2} + M_{C3}) \end{bmatrix} \begin{bmatrix} \dot{u} \\ \dot{q} \\ u \end{bmatrix} + \begin{bmatrix} M & I \\ S^T M & S^T \end{bmatrix} \begin{bmatrix} g \\ f \end{bmatrix} \quad (22)$$

Then, taking  $x = [\dot{u} \ \dot{q} \ u \ q]$  as the augmented state vector, and rearranging the matrices, the system expressing the dynamics of the mechanism can be written also as:

$$\begin{bmatrix} M & MS & 0 & 0 \\ S^T M & S^T MS & 0 & 0 \\ 0 & 0 & I & 0 \\ 0 & 0 & 0 & I \end{bmatrix} \begin{bmatrix} \ddot{u} \\ \ddot{q} \\ \dot{u} \\ \dot{q} \end{bmatrix} = \begin{bmatrix} -2M_G - \alpha M - \beta K & -MS & -(M_{C1} + 2M_{C2} + M_{C3}) - K & 0 \\ S^T(-2(M_{G1} + M_{G2}) - \alpha M) & -S^T MS & -S^T(M_{C1} + 2M_{C2} + M_{C3}) & 0 \\ I & 0 & 0 & 0 \\ 0 & I & 0 & 0 \end{bmatrix} \begin{bmatrix} \dot{u} \\ \dot{q} \\ u \\ q \end{bmatrix} + \begin{bmatrix} M & I \\ S^T M & S^T \\ 0 & 0 \\ 0 & 0 \end{bmatrix} \begin{bmatrix} g \\ f \end{bmatrix} \quad (23)$$

The values of acceleration can be computed at each step by solving the Equation 22, while the values of velocities and of displacements can be obtained by an appropriate integration scheme (e.g. the Runge-Kutta algorithm) and, hence, the dynamic behaviour of the system can be simulated.

## 3 REFERENCE MECHANISM

The model presented in the previous section is valid for any spatial mechanism with any number of free coordinates. Hence, an L-shape mechanism is chosen as the basis of the simulation. The mechanism is made by two steel rods, connected by a rigid aluminium joint. The kinematics and dynamics characteristics of the reference mechanism are reported in Table I.



Figure 2 the mechanism built in the laboratory for the experimental validation of the model

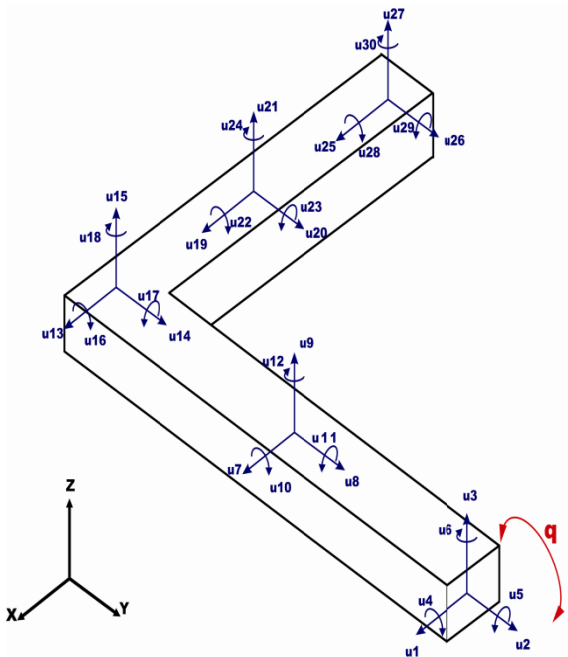


Figure 3 Elastic displacement in the L-shape mechanism

Each beam finite element in the spatial environment has 12 degrees of freedom. According to Figure 3, the mechanism has been discretized using 4 beam elements. After assembling them and considering the constraints imposed by the kinematic couplings and neglecting one of the nodal displacements in order to make the system solvable [15], the resulting flexible system is described by 24 nodal elastic displacements and one rigid degree of freedom.

Table I - Kinematics and dynamics characteristic of the reference mechanism

	Symbol	Value
Young's modulus	E	$2 \times 10^{11}$ [Pa]
Flexure inertia moment	J	$11.102 \times 10^{-10}$ [m <sup>4</sup> ]
Poisson's coefficient	$\nu$	0.33
Beam width	a	$30 \times 10^{-3}$ [m]
Beam thickness	b	$10 \times 10^{-3}$ [m]
Density	$\rho$	$2.7 \times 10^3$ [Kg/m <sup>3</sup> ]
First link length	L <sub>1</sub>	0.5 [m]
Second link length	L <sub>2</sub>	0.5 [m]
Rayleigh damping constant	$\alpha$	$7 \times 10^{-4}$ [s <sup>-1</sup> ]
	$\beta$	$2.13 \times 10^{-7}$ [s]

#### 4 LINEAR STATE-SPACE DYNAMIC MODEL

In order to develop a state-space linear model, to be used as the prediction model for a linear MPC controller, a linearization procedure has been applied to the differential Equation 22 which is nonlinear due Coriolis term and to the effects of gravity. Gasparetto has presented linearization procedure that can be applied to planar mechanisms in [16]. A similar procedure is applied here, by extending it also to spatial mechanisms.

From the basics of linear system theory, a linear time-invariant (LTI) model in state space form can be written as:

$$\begin{cases} \dot{x}(t) = F_{lin}x(t) + G_{lin}v(t) \\ y(t) = H_{lin}x + D_{lin}v(t) \end{cases} \quad (24)$$

where  $x(t)$ ,  $y(t)$  and  $v(t)$  represents the state vector, output vector and input vector respectively and  $F_{lin}$ ,  $G_{lin}$ ,  $H_{lin}$  and  $D_{lin}$  are time-invariant matrices. Considering  $x = [\dot{u}, \dot{q}, u, q]^T$  as the state vector, linearized state-space form of the dynamic model of Equation 23 can be reported as:

$$A_{lin}\dot{x} = B_{lin}x + C_{lin}\tau \quad (25)$$

Taking into account the equilibrium point  $x_e$  in the mechanism configuration and choosing  $u = u_e$  under the system input  $v = v_e$  in the proximity of the equilibrium point, the following equation can be considered:

$$\begin{cases} x(t) = x_e + \Delta x(t) \\ v(t) = v_e + \Delta v(t) \end{cases} \quad (26)$$

By substituting the above relations into Equation 23, the following relation can be found:

$$A_{lin}(x_e)\Delta\dot{x} = B_{lin}(x_e + \Delta x)(x_e + \Delta x) + C_{lin}(x_e + \Delta x)(v_e + \Delta v) \quad (27)$$

After some mathematical operations, the constant  $A_{lin}$  and  $B_{lin}$  matrices in Equation 24 can be evaluated as:

$$A_{lin} = \begin{bmatrix} M & MS & 0 & 0 \\ S^T M & S^T MS & 0 & 0 \\ 0 & 0 & I & 0 \\ 0 & 0 & 0 & I \end{bmatrix}_{x=x_e} \quad (28)$$

$$B_{lin} = \begin{bmatrix} -2M_G - \alpha M - \beta K & 0 & -K & B_{14} \\ S^T(-2M_G - \alpha M - \beta K) & 0 & 0 & B_{24} \\ I & 0 & 0 & 0 \\ 0 & I & 0 & 0 \end{bmatrix}_{x=x_e} \quad (29)$$

in which:

$$B_{14} = -\frac{\partial K}{\partial q} \cdot \frac{K}{F_g} + \frac{\partial F_g}{\partial q} \quad (30)$$

$$B_{24} = \frac{\partial S^T}{\partial q} \cdot F_g + S^T \cdot \frac{\partial F_g}{\partial q} \quad (31)$$

where  $F_g$  represents the gravity force.

$C_{lin}$  is unaltered by the linearization procedure since is composed of only zeroes and ones. Finally, the standard the state-space form of  $A_{lin}$ ,  $B_{lin}$  and  $C_{lin}$  can be easily extracted:

$$\begin{cases} \Delta \dot{x} = F_{lin} \Delta x + G_{lin} \Delta v \\ y = H_{lin} x + D_{lin} v \end{cases} \quad (32)$$

where:

$$\begin{aligned} F_{lin} &= A_{lin}^{-1} B_{lin} \\ G_{lin} &= A_{lin}^{-1} C_{lin} \end{aligned} \quad (33)$$

#### 4.1 Accuracy of the linearized Model

In this subsection, a simple comparison test in order to evaluate the extracted accuracy linearized model has been described. The mechanism, introduced in section 3, has been fed with 5 Nm torque impulse with 0.05 sec delay in the initial configuration of  $q_0 = 90^\circ$ , i.e. starting from the vertical position; however, it should be mentioned that the test can be implemented to any mechanism configuration with similar results.

From the Figure 4 and 5 it can be inferred that linearized model has a very high level of precision as well as the rotation motion of  $q$  is considered. As can be seen from the Figure 4, the response of the linear and nonlinear models of  $q$  as the generalized coordinate is very close and similar to each other; however, the difference between them increases when moves away from the equilibrium point. Additionally, it can be inferred from Figure 5 that the error on  $q$  increases slowly as the error after 0.4 s is around 0.06%.

Figure 6 shows a comparison of the responses of nonlinear and linearized system impulsive on the subject of nodal displacements  $u_{11}$ . According to Figures 6, the difference between the linear and nonlinear modelling of  $u_{11}$  are negligible while the mechanism moves from the equilibrium configuration as far as  $u_{11}$  is concerned. Figures 7 shows the modelling error on  $u_{11}$ , which is very small at beginning of the motion and grows slowly during the mechanism manoeuvre.

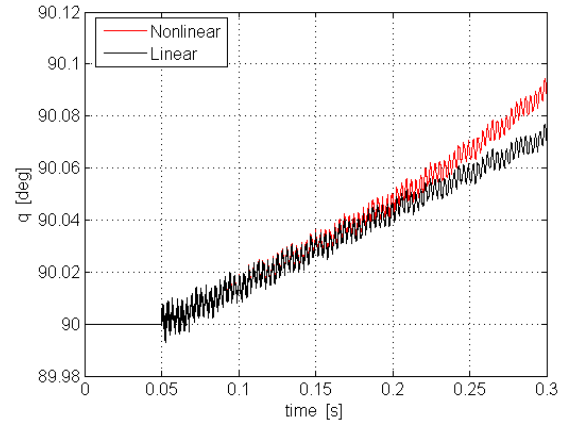


Figure 4 Comparison between linear and nonlinear impulsive response: angular position  $q$

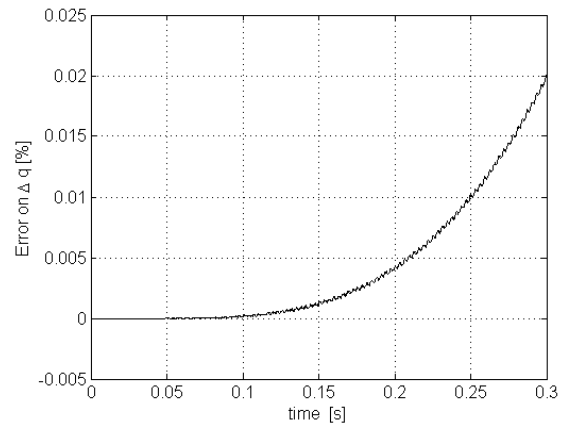


Figure 5 Comparison between linear and nonlinear impulsive response: percentage error on angular position  $q$

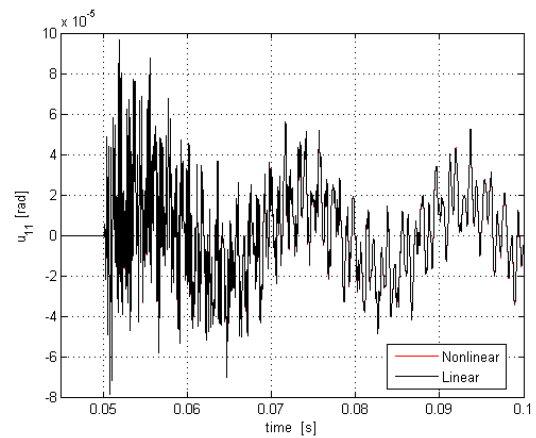


Figure 6 Comparison between linear and nonlinear impulsive response: elastic displacement  $u_{11}$

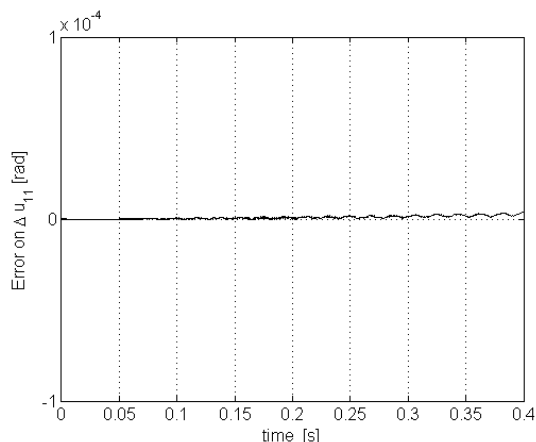


Figure 7 Comparison between linear and nonlinear impulsive response: error in radian on elastic displacement  $u_{11}$

#### 4.2 State Observer

Fundamentally, a state observer estimates the state variables by means of measuring a subset of the output and control variables in order to reconstruct the state of a system where the measurement is difficult or even impossible in some specific situations.

A brief explanation of the Kalman observer used in our system, is summarized here. For more details about methodology and designing refer to [17].

Basically an observer design depends upon on two basis, a linear time invariant dynamic model of the system and linear relation between the state variables and the sensed outputs. The dynamic of the overall system is described very briefly by the following system of equations:

$$\Delta \hat{x} = F \Delta \hat{x} + G \Delta u + L(\Delta y - \Delta \hat{y}) \quad (34)$$

$$\hat{y} = H \Delta \hat{x} \quad (35)$$

$$\Delta z = -W \Delta \hat{x} \quad (36)$$

$$e = \Delta \hat{x} - \Delta x \quad (37)$$

where  $e$  and  $L$  are the vector of the errors of the state variable estimates ( $\hat{x}$ ) and the time invariant gain matrix of the asymptotic Kalman estimator, respectively.

Additionally  $W$  is the time invariant gain vector of linear regulator and  $F$  and  $H$  matrices are used to assess the system observability as well. The control vector is shown by  $u$  while  $y$  and  $\hat{y}$  present the real output signals and estimated ones respectively.  $G$  is a matrix which is related to the linearized model of the equilibrium configuration. However, it should be noticed that these equations only hold in the neighbourhood of an equilibrium configuration.

In order to evaluate our system observer, a similar test described in the previous subsection with the same input and configuration has been implemented. In this test knowledge about nodal displacement  $u_{19}$  and generalized coordinate  $q$  are available by the measurement in the purpose of estimating all states of the system.

From the Figure 8 and 9, it can be concluded that the Kalman observer has a good accuracy for estimating the generalized coordinate  $q$  as a one system state. Regarding the Figure 8, the impulsive response of nonlinear and observer are very similar; although, more far from the equilibrium point, more differences among the responses. Particularly, Figure 9 shows the error on  $q$  that is, after 0.4 sec the error between nonlinear and estimator is still so small and converge to zero.

Figure 10 illustrates the comparison between the impulsive respond of actual measurement of displacement  $u_{19}$  and estimated  $u_{19}$  by Kalman observer. As it can be seen from Figure 11 the difference is not so significant during the transient. Nevertheless they increase as the mechanism moves from the equilibrium configuration. In particular the difference on  $u_{19}$  between the nonlinear system and the observer are so small as long as the motion from the original position is kept.

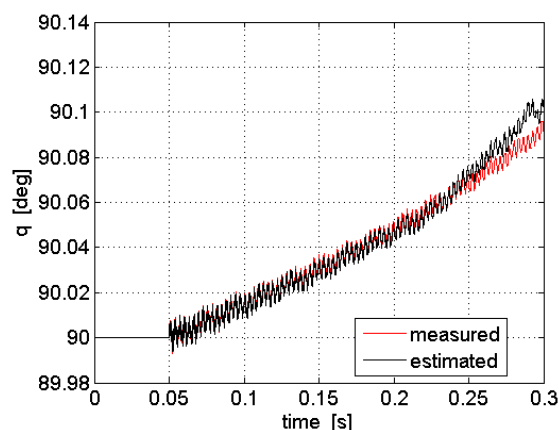


Figure 8 Comparison between measured and estimated angular position  $q$

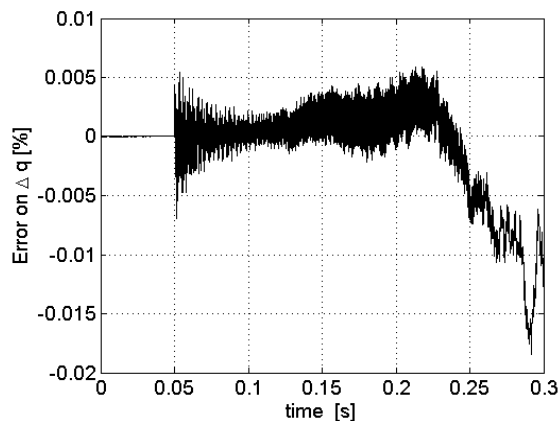


Figure 9 Percentage error on estimation of angular position  $q$

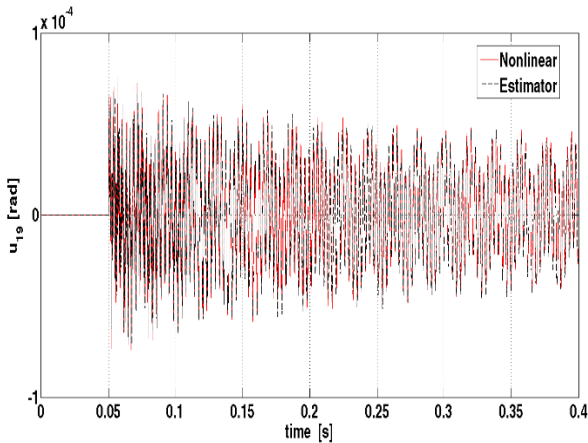


Figure 10 Comparison between response of impulsive response of nonlinear and estimated  $u_{19}$

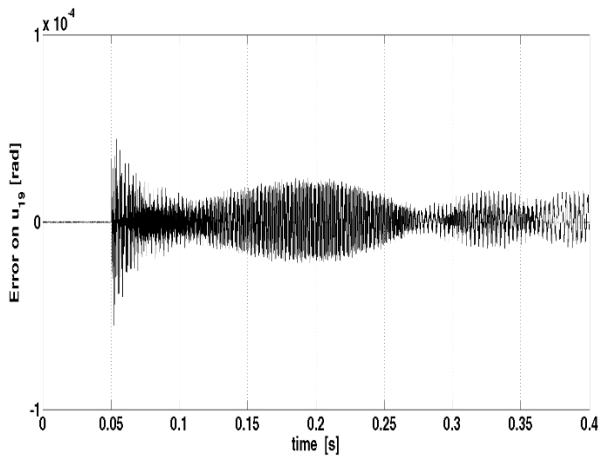


Figure 11 error in radian on estimation of elastic displacement  $u_{19}$

## 5 MODEL PREDICTIVE CONTROL WITH CONSTRAINT

In this section a short introduction to constrained MPC is given. Model Predictive Control (MPC) is a class of computer control algorithms that is based on constructing controllers that are able to adjust the control action before a variation in the occurrence of the output set point. At each control interval the MPC algorithm attempts to optimize future plant performance by computing a sequence of future manipulated variable adjustment. An MPC algorithm can be tuned according to a cost function, constraints on controlled and control variables and to a model of the process to be controlled. For further reading on constrained MPC see [18].

### 5.1 Prediction and Control Horizons

Prediction horizon  $H_p$  is the number of samples over which a prediction of the plant outputs is evaluated at each iteration of the controller, while control horizon  $H_c$  is the

number of samples over which the control variables can change their value.

As it can be seen in Figure 12, the MPC controller performs a prediction from current time step  $k$  to the future time step  $k+H_p$ . In the same figure it is shown that the control action can change only over the time interval  $[k, k+H_c]$ . The control action is chosen in order to minimize a given cost function. The first value of the optimal control sequence is actually fed to the plant, and the whole calculation is repeated at subsequent control intervals. Prediction horizon is moving forward for every iteration in time and the MPC controller predicts the plant output again.

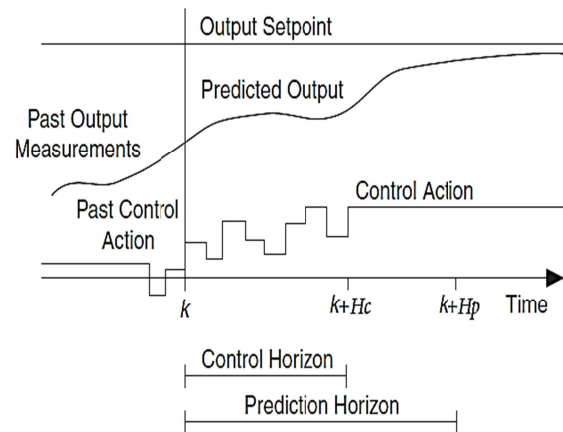


Figure 12 A discrete MPC controller scheme

### 5.2 Model Prediction and Cost Function

A discrete time state-space model is often used to provide predictive capability in MPC controller:

$$x_{k+1} = Ax_k + Bw_k \quad (38)$$

$$y_k = Cx_k + Dw_k \quad (39)$$

The MPC controller computes a sequence of the predicted new control input vector in order to minimize a cost function. Often used cost function in MPC is the linear quadratic function:

$$J = \sum_{k=0}^{H_p} (\hat{y} - r)^T Q (\hat{y} - r) + \sum_{k=0}^{H_c} \Delta w^T R_1 \Delta w + \sum_{k=0}^{H_c} w^T R_2 w \quad (40)$$

in which  $\hat{y}$ ,  $r$ ,  $\Delta w$ ,  $w$  are the predicted plant outputs, the reference signal for outputs, the change rate of control action and the control action, respectively.  $Q$ ,  $R_1$  and  $R_2$  are the weighting matrices used to tune the control performance.  $Q$  is used to penalize the tracking error, while  $R_1$  and  $R_2$  are used to penalize the change rate and the absolute value of control action, respectively. In general, Equation 40 is used in MIMO systems (Multiple Input and Multiple Outputs) and also could be expanded to MISO systems (Multiple Input and Single Output) such as our case, a system with 50 inputs (states) and one output (torque).

Constrained MPC controller has ability to take into account constraints of physical systems in its future control performance calculations. The formulation used in this paper allows to define constraints as follows:

$$y_{min} \leq y \leq y_{max} \quad (41)$$

And inputs constrains can be defined as:

$$\Delta w_{min} \leq \Delta w \leq \Delta w_{max} \quad (42)$$

$$w_{min} \leq w \leq w_{max} \quad (43)$$

## 6 RESULT OF MODEL PREDICTIVE CONTROL WITH CONSTRAINT

In this section the results of several numerical tests are provided and discussed to show the capabilities of the MPC controller for position and vibration control of flexible mechanisms. The tuning of the MPC controller depends on weight on  $u_{12}$ , weight on  $q$ , sampling time ( $T_s$ ), prediction horizon ( $H_p$ ) and control horizon ( $H_c$ ).

In practical applications, the values of  $T_s$ ,  $H_p$  and  $H_c$  should be selected on the basis of the available computational resources. The computational cost of solving the optimization problem of each iteration of the controller depends on both  $H_p$  and  $H_c$ .

Generally speaking, longer  $H_c$  results in aggressive control action while longer  $H_p$  causes more damped response and more precise reference tracking [12].

The whole behaviour of the controller relies on a large set of variables. Constraints on actuation torque are chosen to comply with the physical limitations of the actuator. Other parameters can be tuned quite freely. In this case, constraints can be imposed on elastic displacement ( $u$ ), angular position ( $q$ ) and input torque ( $\tau$ ) as:

$$u_{k_{min}} \leq u_k \leq u_{k_{max}}, k = 1 \dots 24 \quad (44)$$

$$q_{min} \leq q \leq q_{max} \quad (45)$$

$$\tau_{min} \leq \tau \leq \tau_{max} \quad (46)$$

It should be mentioned that in our system just the constraint on torque, which is  $-8 \leq \tau \leq 8$  Nm, is active.

In the following the effects of choosing different values for tuning parameters of MPC controlled are discussed by means of numerical tests.

### 6.1 Effects of $f_c$ on the Closed-loop System

Figure 13 and 14 demonstrate the response of angular position  $q$  and elastic displacement  $u_{12}$  with different sampling frequency. In all the tests reported in this work, the mechanisms performs a 30 degree of rotation in counter-clockwise direction starting from the horizontal position.

It can be seen from Figure 13 that the performance of the angular position response for both values of sampling frequency 100 Hz and 1kHz are very similar; however, it should be mentioned that the values of  $H_p$  and  $H_c$  are chosen 20 and 5 for  $f_c = 100$  Hz and 200 and 50 for  $f_c=1$ kHz, respectively. The vibration amplitude for the system with  $f_c=100$  Hz is bigger than the system with  $f_c=1$

kHz during the transient as it is depicted in Figure 14 for elastic displacement  $u_{12}$ . The more effective vibration damping achieved by the 1 kHz control can be explained by taking into consideration the faster control has a sufficient bandwidth to take into account all the significant vibration modes of the flexible mechanism.

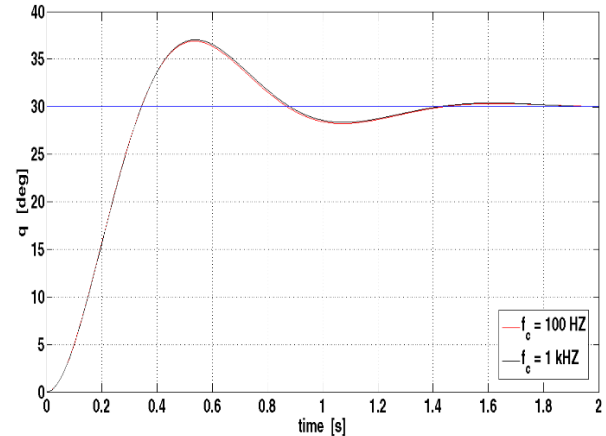


Figure 13 Response of the Angular position  $q$  at with different sampling frequency, 1 kHz and 100 kHz

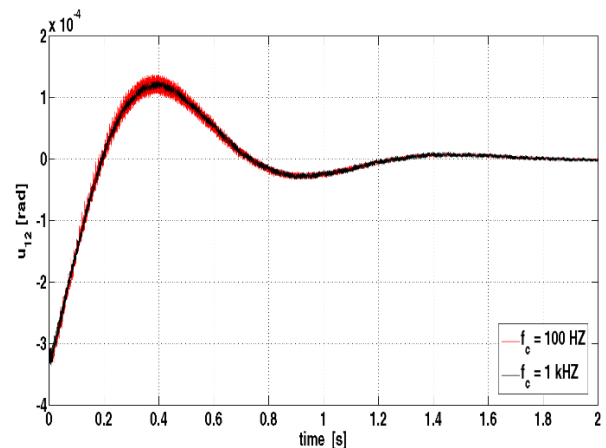


Figure 14 Effect analysis of different sampling frequency ( $f_c$ ) on the elastic displacement  $u_{12}$

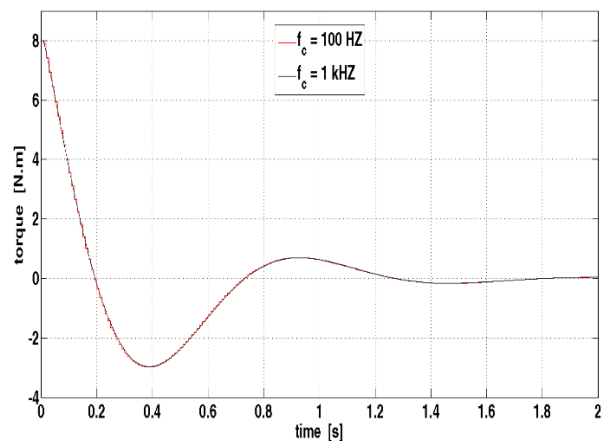


Figure 15 Applied torque to the mechanism

From the Figure 15 it can be inferred that applied torque by the control system is within the range defined by the constraint.

### 6.2 Effects of $H_c$ and $H_p$ on the Closed-loop System

In Figure 16 and 17 the effects of choosing different control horizon has been investigated. It can be inferred that tuning the  $H_c$  parameter has a limited effect on the response of the closed loop system. Consequently,  $H_c$  can be increased up to  $H_p$  but the performance of the controller will not be improved significantly. In most cases  $H_c$  should be kept quite small, since a longer control horizon increases the computational effort required to solve the minimization problem defined by Equations 38-40.

Regarding Figure 18 and 19, changing the value of the prediction horizon ( $H_p$ ) has a significant effect on the performance of the controller. As it can be inferred from Figure 18, selecting bigger value for  $H_p$  causes more damped response for angular position  $q$ ; conversely, smaller value for  $H_p$  result in more aggressive response. A similar consideration can be achieved by analysing the Figure 19, which reports the time evolution of elastic displacement  $u_{12}$ .

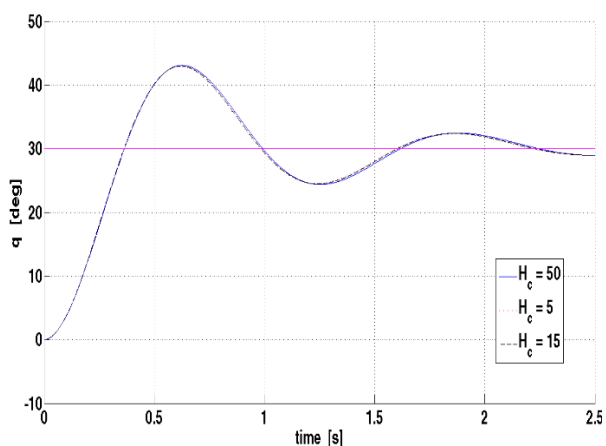


Figure 16 Effect analysis of different control horizon ( $H_c$ ) on angular position  $q$

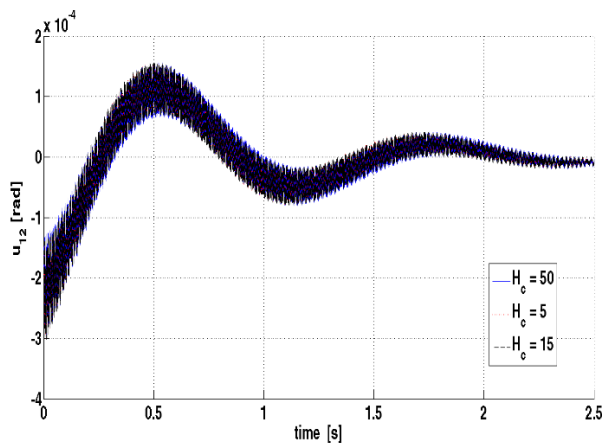


Figure 17 Effect analysis of different control horizon ( $H_c$ ) on elastic displacement  $u_{12}$

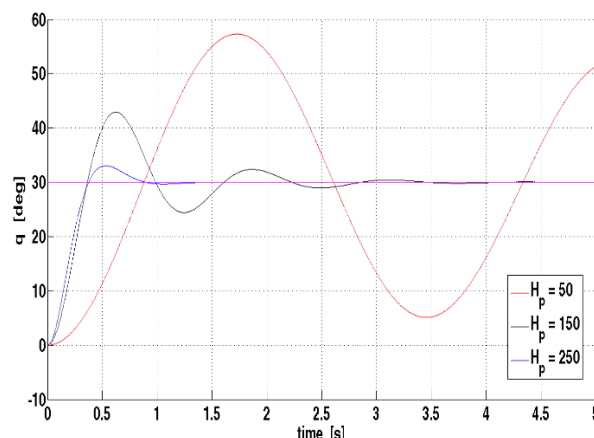


Figure 18 Effect analysis of different control horizon ( $H_p$ ) on angular position  $q$

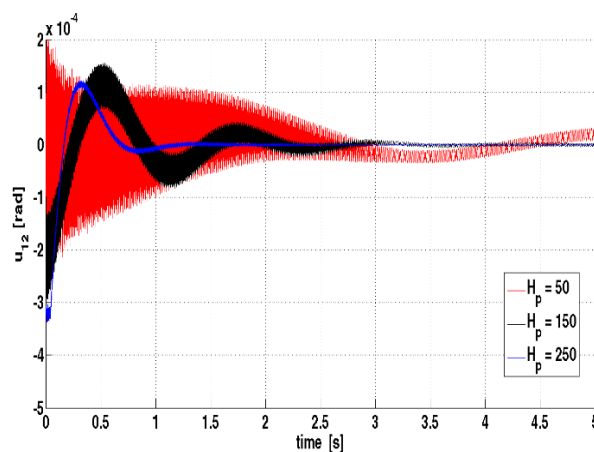


Figure 19 Effect analysis of different control horizon ( $H_p$ ) on elastic displacement  $u_{12}$

Again, higher values of the prediction horizon leads to a higher damping of vibrations.

Therefore we can conclude that the prediction horizon should be set as high as the computational resources allows it. Since the performance of the closed-loop system are less sensitive to the choice of the control horizon,  $H_c$  can be set to a low value to reduce the computational effort required to solve the optimization problem.

## 7 ROBUSTNESS

In this section the results of two tests which are implemented in order to evaluate robustness of the proposed control scheme are discussed.

Several simulations have been performed with applying the same control system on the nonlinear model with different parameters. The tests have been done with uncertainties of different sign (i.e. +20%, -20%) on the mechanism links lengths ( $L=L_1+L_2$ ) and on the Young's elastic modulus  $E$ .

These tests that have been developed in order to evaluate the robustness properties of the proposed control scheme, using an approach already reported in other works such as [14,19].

In Figure 20 the effects of changing the mechanism length ( $L=L_1+L_2$ ) of the mechanism have been shown. According to the Figure 20, the tolerance in the mechanism length does not bring the closed loop to instability. If the actual length of the links is 20% larger than the nominal value, the response of the system will be more damped. On the other hand, by decreasing by 20% the mechanism length, the overshoot of angular position  $q$  is increased with respect to the nominal case.

Thus it can be inferred that the developed controlled is quite robust to this kind of uncertainty, as far as angular position tracking is concerned. It can be seen in Figure 21 that also vibration damping is influenced by mismatches in mechanism length. If mechanism length is under-estimated, a more effective vibration damping can be achieved, since the overall response of the closed-loop system is slower.

According to Figure 22 and 23, changing the value of elastic modulus  $E$  of a  $\pm 30\%$  does not alter significantly the performance of the control scheme, thus the designed MPC controller is also robust respect to changes in the vibration models of the plant.

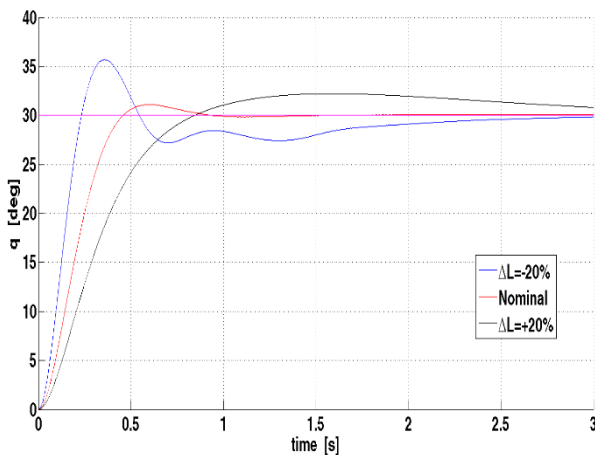


Figure 20 Robustness analysis of the change in the mechanisms links lengths ( $L=L_1+L_2$ ) on angular position  $q$

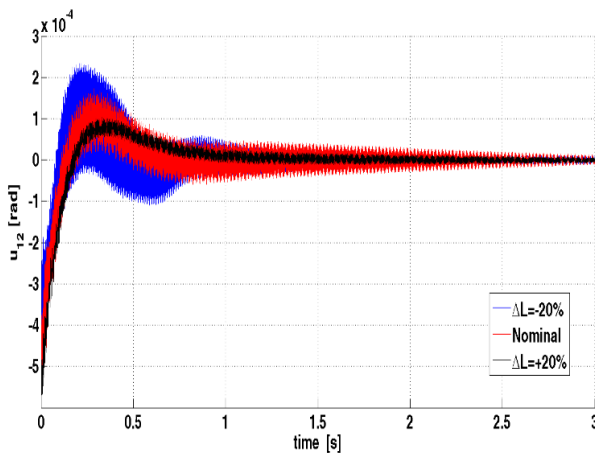


Figure 21 Robustness analysis of the change in the mechanisms links lengths ( $L=L_1+L_2$ ) on elastic displacement  $u_{12}$

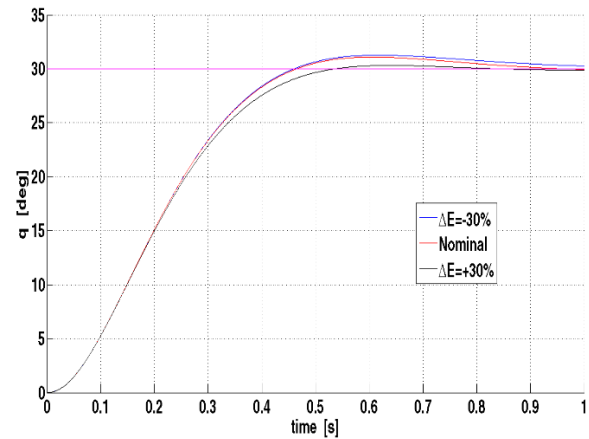


Figure 22 Robustness analysis of the change of elastic modulus  $E$  on angular position  $q$

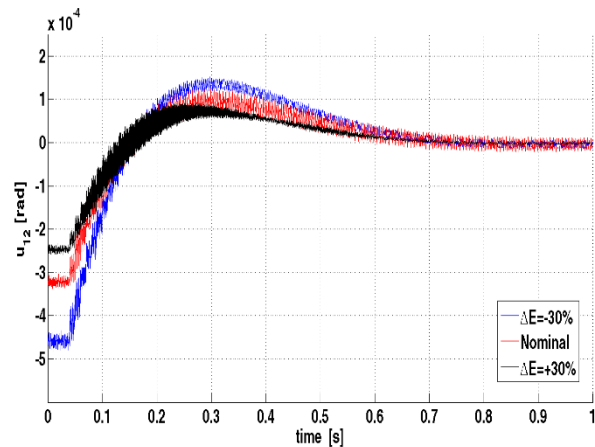


Figure 23 Robustness analysis of the change of elastic modulus  $E$  on elastic displacement  $u_{12}$

## 8 MPC CONTROLLER VS. PID CONTROLLER

In this section a comparison between results of MPC and PID controller has been made and discussed. While PID controller are applied in single loop controllers, MPC controller are used for overall system. PID controllers support only a single input put system but MPC are applicable in multi input and multi output systems (MIMO system).

As is shown at Figure 24 PID controller follow the target reference with high speed and low error but with remarkable overshoot ( $\cong 35\%$ ). The tuning of the PID control has been chosen to provide for a similar rise time. Moreover, it can be inferred from the Figure 25 that the amplitude of elastic displacement  $u_{12}$  is significantly larger if a simple PID controller is used.

It can be therefore inferred that in this case MPC control outperforms PID, which is currently the most widely used control technology in industrial applications.

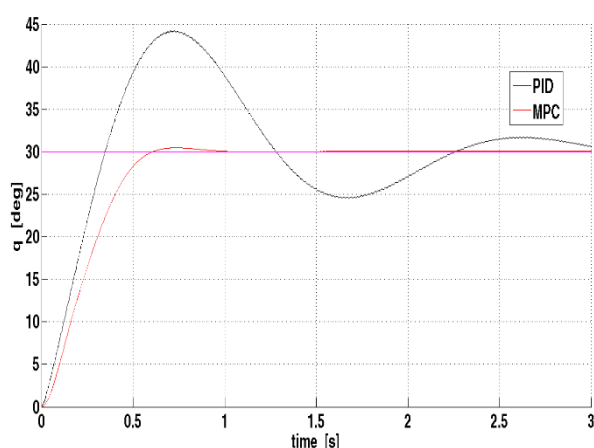


Figure 24 Response of the closed loop system with PID and MPC controller on angular position  $q$

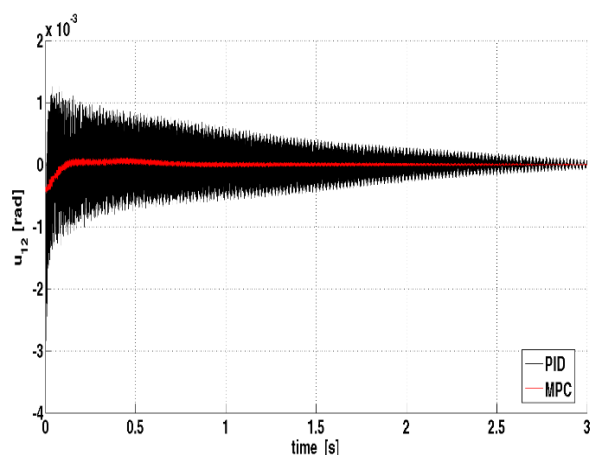


Figure 25 Response of the closed loop system with PID and MPC controller on elastic displacement  $u_{12}$

## CONCLUSION

In this work, a model predictive control with constrains for a 3D L-shape mechanism has been designed and tested. The dynamic behaviour of the flexible mechanism is described by means of a high accurate finite element method, based on the equivalent rigid link system (ERLS) theory and accounting for geometric nonlinearities and gravity force. In order to develop the constrained MPC controller the dynamic model of the mechanism is linearized; accordingly, a Kalman state observer has been developed as well. The proposed control scheme allows to minimize a performance index which takes into consideration both the amplitude of vibrations and the angular position of the mechanism. Meanwhile two tests on different perturbed plants has been implemented in order to analyse the robustness performance of the proposed control scheme. Finally a comparison between performance of the standard PID controller and MPC controller performance has been done and the results show that MPC controller not only is very effective for both reference position tracking and

vibration suppression but also represent a high level of robustness to uncertainties on the plant.

## REFERENCES

- [1] R. Schwertassek, S. Dombrowski, and O. Wallrapp, "Modal Representation of Stress in Flexible Multibody Simulation," *Nonlinear Dyn.*, vol. 20, no. 4, pp. 381–399, 1999.
- [2] O. A. Bauchau, "Flexible Multibody Dynamics," Springer, 2011.
- [3] M. Giovagnoni, "A Numerical and Experimental Analysis of a Chain of Flexible Bodies," *J. Dyn. Syst. Meas. Control*, vol. 116, no. 1, pp. 73–80, Mar. 1994.
- [4] A. Shabana, "Flexible Multibody Dynamics: Review of Past and Recent Developments," *Multibody Syst. Dyn.*, vol. 1, no. 2, pp. 189–222, 1997.
- [5] O. Tokhi and A. K. M. Azad, *Flexible Robot Manipulators: Modelling, Simulation and Control*. Institution of Engineering and Technology, 2008.
- [6] S. K. Dwivedy and P. Eberhard, "Dynamic analysis of flexible manipulators, a literature review," *Mech. Mach. Theory*, vol. 41, no. 7, pp. 749–777, Jul. 2006.
- [7] S. S. Ge, T. H. Lee, and G. Zhu, "A nonlinear feedback controller for a single-link flexible manipulator based on a finite element model," *J. F. Robot.*, vol. 14, no. 3, pp. 165–178, 1997.
- [8] P. Kalra and A. M. Sharan, "Accurate modelling of flexible manipulators using finite element analysis," *Mech. Mach. Theory*, vol. 26, no. 3, pp. 299–313, 1991.
- [9] J. M. Martins, Z. Mohamed, M. O. Tokhi, J. Sa da Costa, and M. A. Botto, "Approaches for dynamic modelling of flexible manipulator systems," *Control Theory and Applications, IEE Proceedings -*, vol. 150, no. 4, pp. 401–411, 2003.
- [10] M. Benosman and G. Le Vey, "Control of flexible manipulators: A survey," *Robotica*, vol. 22, no. 05, pp. 533–545, 2004.
- [11] R. Caracciolo, D. Richiedei, A. Trevisani, and V. Zanotto, "Robust mixed-norm position and vibration control of flexible link mechanisms," *Mechatronics*, vol. 15, no. 7, pp. 767–791, Sep. 2005.
- [12] P. Boscariol and V. Zanotto, "Design of a controller for trajectory tracking for compliant mechanisms with effective vibration suppression," *Robotica*, vol. 30, no. 01, pp. 15–29, 2012.
- [13] S. Kurode and P. Dixit, "Control of tip position of flexible link manipulator using sliding modes," in *2nd Int. Conference on Advances on control and optimization of dynamical systems (ACODS 12)* IISC Bangalore, India, 2012.
- [14] P. Boscariol, A. Gasparetto, and V. Zanotto, "Model Predictive Control of a Flexible Links Mechanism," *J. Intell. Robot. Syst.*, vol. 58, no. 2, pp. 125–147, 2010.
- [15] R. Vidoni, A. Gasparetto, and M. Giovagnoni, "Design and implementation of an ERLS-based 3-D dynamic formulation for flexible-link robots," *Robot.*

- Comput. Integr. Manuf., vol. 29, no. 2, pp. 273–282, Apr. 2013.
- [16] A. Gasparetto, “Accurate Modelling of a Flexible-Link Planer Mechanism by Means of a Linearized Model in The State-space Form for Design of a Vibration Controller,” *J. Sound Vib.*, vol. 240, no. 2, pp. 241–262, Feb. 2001.
- [17] R. Caracciolo, D. Richiedei, and A. Trevisani, “Design and experimental validation of piecewise-linear state observers for flexible link mechanisms,” *Meccanica*, vol. 41, no. 6, pp. 623–637, 2006.
- [18] J. M. Maciejowski, *Predictive Control: With Constraints*. Prentice Hall, 2002.
- [19] N. O. Ghahramani and F. Towhidkhah, “Constrained incremental predictive controller design for a flexible joint robot,” *ISA Trans.*, vol. 48, no. 3, pp. 321–326, Jul. 2009.
- [20] Bossi, L., et al. "Multivariable predictive control for vibrating structures: An application." *Control Engineering Practice* 19.10 (2011): 1087-1098.
- [21] Takács, Gergely, and Boris Rohal'-Ilkiv. *Model Predictive Vibration Control: Efficient Constrained MPC Vibration Control for Lightly Damped Mechanical Structures*. Springer, 2012.
- [22] Boscariol, Paolo, et al. "On the modeling of flexible-link robots: First experimental validation of an ERLS-FEM dynamic model." *Mechatronics (ICM), 2013 IEEE International Conference on*. IEEE, 2013.
- [23] P. Boscariol, A. Gasparetto, and V. Zanotto, “Active Position and Vibration Control of a Flexible Links Mechanism Using Model-Based Predictive Control,” *J. Dyn. Syst. Meas. Control*, vol. 132, no. 1, p. 14506, Dec. 2009.